One-dimensional steady-state model for stimulated Raman and Brillouin backscatter processes in laser-irradiated plasmas

Zhe Yi Ge[1], Guo Bo Zhang[1] ⬤, Yan Zhao Ke[1], Xiao Hu Yang[1,2], Fu Yuan Wu[1], Shi Jia Chen[1] and Yan Yun Ma[1,2]

[1]College of Liberal Arts and Science, National University of Defense Technology, Changsha 410073, China and [2]Collaborative Innovation Center of IFSA (CICIFSA), Shanghai Jiao Tong University, Shanghai 200240, China

Abstract

A one-dimensional steady-state model for stimulated Raman backscatter (SRS) and stimulated Brillouin backscatter (SBS) processes in laser-irradiated plasmas is presented. Based on a novel "predictor-corrector" method, the model is capable to deal with broadband scattered light and inhomogeneous plasmas, exhibiting robustness and high efficiency. Influences of the electron density and temperature on the linear gains of both SRS and SBS are investigated, which indicates that the SRS gain is more sensitive to the electron density and temperature than that of the SBS. For the low-density case, the SBS dominates the scattering process, while the SRS exhibits much higher reflectivity in the high-density case. The nonlinear saturation mechanisms and competition between SRS and SBS are included in our model by a phenomenological method. The typical anti-correlation between SRS and SBS versus electron density is reproduced in the model. Calculations of the reflectivities are qualitatively in agreement with the typical results of experiments and simulations.

Introduction

Stimulated Raman backscatter (SRS) and stimulated Brillouin backscatter (SBS) are crucial issues for laser-driven inertial confinement fusion (ICF) (Lindl *et al.*, 2004). Some of the Nova experiments have shown as much as 35% of the incident laser energy backscattered as SBS (Lindl, 1998). In other experiments, SRS-reflected energy fractions as high as 25% have been observed (Lindl, 1998). Experiments at the National Ignition Facility (NIF) also show that the laser energy scattered through SRS and SBS from the hohlraum is beyond the expectation (Glenzer *et al.*, 2011). The backscattered light can lead to energy loss of the incident laser, and the hot electrons generated by the SRS can preheat the capsule and spoil the implosion symmetry (Kruer, 1988; Powers *et al.*, 1995; Lindl *et al.*, 2004). As a result, the backscattered processes would significantly reduce the energy deposition of the incident beams and increase the laser energy required to drive a target to ignition. Thus, it is urgent to clearly comprehend the detailed physics of the SRS and SBS, and find a way to restrain these instabilities.

In the past decades, lots of theoretical and experimental work have been carried out to investigate the SRS and SBS (Tang, 1966; Rosenbluth, 1972; Pesme *et al.*, 1973; Ramani and Max, 1983; Berger *et al.*, 1998; Boyd and Sanderson, 2003; Hu and Hu, 2003; Hao *et al.*, 2012, 2014; Gong *et al.*, 2013; Amiranoff *et al.*, 2018; Kirkwood *et al.*, 2018; Marques *et al.*, 2019; Peng *et al.*, 2019). Linear theory based on the three-wave interaction model is the most widely used method in analysis of experiments (Hinkel *et al.*, 2008; Neumayer *et al.*, 2008; Froula *et al.*, 2010; Li *et al.*, 2012). Tang (1966) developed the traditional linear theory further by including the pump depletion effect in their model. However, due to the assumption of homogeneous electron density, Tang's model fails for the inhomogeneous plasmas. Strozzi *et al.* (2008) extended the traditional three-wave model to a more robust one, in which the volume noise source by bremsstrahlung and Thomson scattering is considered. According to the new model, the code DEPLETE is developed. Nevertheless, the DEPLETE overestimates the reflectivities of both SRS and SBS because the nonlinear saturation mechanisms are not included in the code. Peng *et al.* (2019) also present the recent progress in the strong-coupling regime of Brillouin scattering (sc-SBS), which describes the role of the global phase in the spatio-temporal equations for backscattering. Recently, several models that focus on the competition mechanism between SRS and SBS have been proposed with more physical processes than the DEPLETE (Gong *et al.*, 2013; Hao *et al.*, 2014). However, the efficiencies of these models are limited since the complicated coupling equations of the pump laser and scattered light with various noise sources need to be solved. Thus, a generally applicable, quantitative model which can describe the SRS and SBS process simultaneously with high efficiency and less computationally expensive is still lacking.

In this paper, we propose a one-dimensional steady-state model to describe the SRS and SBS processes simultaneously in laser-irradiated plasmas. With high efficiency and robustness, the model is capable to deal with broadband scattered light. Pump depletion, boundary noise sources, and inverse-bremsstrahlung damping effects are self-consistently included. A phenomenological method is proposed to include the nonlinear saturation mechanisms and the competition effect between SRS and SBS in our model, and reasonable reflectivity can be obtained. Compared with the traditional Tang's model, our model is also valid for the inhomogeneous plasma case. Besides, much higher efficiency is exhibited in our model than in the DEPLETE model since the solving of a two-point boundary value problem via a shooting method is avoided. Based on the model, we investigate the influences of the electron density and temperature on the linear gains of both SRS and SBS. The anti-correlation between SRS and SBS versus electron density is analyzed in detail. Qualitatively agreement with the typical results of experiments and simulations demonstrates the effectiveness of our model.

This paper is structured as follows. In Section "Theoretical model", the detail theoretical model is presented. Detailed discretized algorithm of our model is illustrated in the "Discretized algorithm" section. The typical numerical results are exhibited in the "Numerical results" section. Section "Nonlinear saturation and competition between SRS and SBS" deals with the nonlinear saturation and competition between SRS and SBS. Furthermore, the comparison of the model with the experimental results is also displayed. Finally, we summarize the results and give the conclusions in the last section.

Theoretical model

In our model, we consider a one-dimensional static plasma slab which locates between $x = 0$ and $x = L$. The pump laser pulse is supposed to incident into the plasma from the left side ($x = 0$), while the scattered light reflects from the opposite boundary ($x = L$). Only backward scattering is dealt with in this article. Customarily, we define I_i as the intensity of light with the frequency ω_i and the wave number k_i, where the subscript $i = 0, s$ for incident and backscattered light, respectively. To describe the broadband scattered light, the intensity is defined as $I_s(x) = \int i_s(\omega_s, x)\, d\omega_s$, where i_s is the spectral density (intensity per angular frequency). Following the DEPLETE model (Strozzi *et al.*, 2008), as well as Gong *et al.* (2013), the coupled intensity equations between the pump and scattered light for the steady state in strong damping limit can be described by

$$\frac{\partial I_0}{\partial x} = -\frac{\omega_0}{\omega_s}\Gamma I_0 I_s, \tag{1}$$

$$\frac{\partial I_s}{\partial x} = -\Gamma I_0 I_s, \tag{2}$$

where the coupling coefficient Γ is

$$\Gamma = \frac{e^2}{2\varepsilon_0 m_e^2 c^4}\frac{k^2}{\omega_0 k_0 k_s}\text{Im}\left[\frac{\chi_e(1+\chi_i)}{1+\chi_e+\chi_i}\right], \tag{3}$$

where e, ε_0, m_e, c denote the electron charge, vacuum permittivity, electron mass, and speed of light, respectively. k is the wave

number of the Langmuir wave for the SRS and the ion acoustic wave for the SBS, respectively. $\chi_e(\chi_i)$ is the electron (ion) susceptibility. For a Maxwellian distribution, the electron susceptibility χ_e is given by

$$\chi_e = -\frac{1}{2k^2\lambda_{\text{De}}^2}Z'(\xi_e), \tag{4}$$

where $\lambda_{\text{De}} = \upsilon_{\text{te}}/\omega_{\text{pe}}$ denotes the Debye length of electrons, $\upsilon_{\text{te}} = \sqrt{T_e/m_e}$ is the electron thermal velocity, $\omega_{\text{pe}} = \sqrt{n_e e^2/\varepsilon_0 m_e}$ means the electron plasma frequency. T_e and n_e are the electron temperature and density, respectively. The plasma dispersion function (Fried and Conte, 1961) is

$$Z(\xi_e) = i\pi^{1/2}e^{-\xi_e^2}\text{erfc}(-i\xi_e), \tag{5}$$

where erfc is the complimentary error function (Abramowitz and Stegun, 1970). $\xi_e = \omega'/\sqrt{2}k\upsilon_{\text{te}}$, and $\omega' = \omega - \vec{k}\cdot\vec{u}$ is the frequency of the Doppler-shifted Langmuir wave due to the plasma speed $\vec{u}$. The total ion susceptibility χ_i is

$$\chi_i = \sum_j \chi_j, \tag{6}$$

where the susceptibility for the ion species j is given by

$$\chi_j = -\frac{1}{2k^2\lambda_{\text{D}j}^2}Z'(\xi_j), \tag{7}$$

where $\lambda_{\text{D}j} = \upsilon_{\text{t}j}/\omega_{\text{p}j}$, $\upsilon_{\text{t}j} = \sqrt{T_j/m_j}$, $\omega_{\text{p}j} = \sqrt{n_j Z_j^2 e^2/\varepsilon_0 m_j}$. T_j, n_j, and Z_j are the temperature, density, and charge state of ion species j, respectively. $\xi_j = \omega'/\sqrt{2}k\upsilon_{\text{t}j}$, and $\omega' = \omega - \vec{k}\cdot\vec{u}$ is the frequency of the Doppler-shifted ion acoustic wave.

Based on Eqs (1) and (2), the intensity of the scattered light at the left boundary ($x = 0$) is derived as follows:

$$I_s(0) = I_s(L) \times e^G, \tag{8}$$

where the linear gain exponent G is defined as

$$G = \int_0^L \Gamma I_0\, dx. \tag{9}$$

Replacing the Γ in Eq. (9) via Eq. (3) yields

$$G = \int_0^L \frac{I_0 e^2}{2\varepsilon_0 m_e^2 c^4}\frac{k^2}{\omega_0 k_0 k_s}\text{Im}\left[\frac{\chi_e(1+\chi_i)}{1+\chi_e+\chi_i}\right]dx. \tag{10}$$

Applying Tang's model (Tang, 1966) directly, the reflectivity R of SRS or SBS, as a function of the gain G, can be obtained by

$$\varepsilon = \frac{R(1-R)}{e^{G(1-R)} - R}, \tag{11}$$

with an initial seed value for the backscattered light of $\varepsilon = 1 \times 10^{-9}$.

Discretized algorithm

The system of equations from Eqs (1) to (11) will be discretized in one-dimensional space using a staggered grid with N cells having
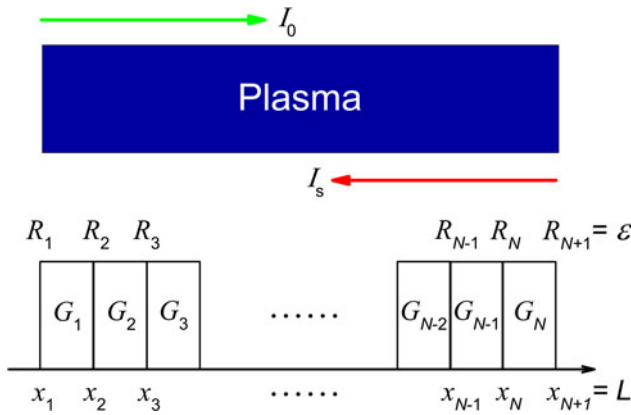
Fig. 1. Schematic of the model and staggered grid.

Fig. 2. The gain exponent of SRS as a function of the scattered light frequency (normalized by the pump laser frequency ω_0) for $n_e/n_c = 0.05$ (black dashed), $n_e/n_c = 0.1$ (blue dotted), and $n_e/n_c = 0.15$ (red solid), respectively.

$N + 1$ boundaries (see Fig. 1). Cell j is located between interface j and $j + 1$, while interface j separates cell $j - 1$ from cell j. In general, G, T_e, n_e, T_j, n_j, and Z_j are defined at cell centers, I_0, I_s, R, and x are defined at interface.

Different from Strozzi et al. (2008), who solved the equation system via a shooting method, we propose a novel "predictor-corrector" method in our model. The algorithms of the model proceed in two steps: firstly, the "prediction" step. Based on the plasma parameters (T_e, n_e, T_j, n_j, Z_j, and I_0), the gain exponent G in each cell is calculated by Eq. (10). The total gain G_{all} is obtained by adding contributions from all the cells:

$$G_{all} = \sum_{j=1}^{N} G_j. \tag{12}$$

The total reflectivity of the backscattered light (the reflectivity at the first interface R_1) can be derived from Eq. (11). Then, we define the gain deviation of the backscattered light as

$$\Delta G = (\ln R_1 - \ln \varepsilon) - G_{all}. \tag{13}$$

Secondly, the "corrector" step. We revise the gain exponent G in each cell by

$$G'_j = G_j + \frac{G_j}{G_{all}} \Delta G. \tag{14}$$

The reflectivity of the backscattered light at each interface R_j can be derived from

$$\ln R_j - \ln R_{j+1} = G'_j, \tag{15}$$

marching from the right to left boundary. The above calculation is suitable for both SRS and SBS. For the pump laser intensity at each interface I_{0j}, the energy conservation reads

$$1 - R_1^{SRS} - R_1^{SBS} = I_{0j} - R_j^{SRS} - R_j^{SBS}. \tag{16}$$

Now, the system of equations is closed, and all the quantities are solved. One can prove that, for the homogeneous plasma, the reflectivity derived by the "predictor-corrector" method will
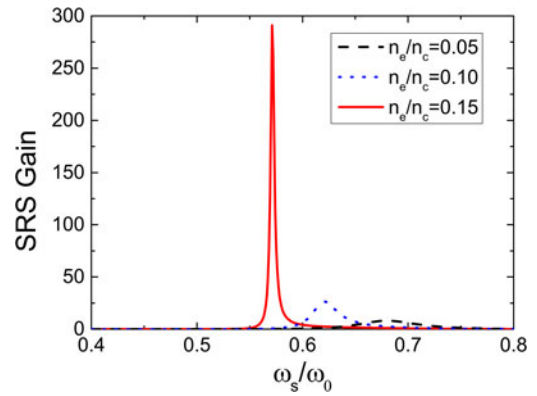
be the same as the Tang's model:

$$\ln R'_1 = G'_1 + \cdots + G'_N + \ln \varepsilon = G_{all} + \Delta G + \ln \varepsilon$$
$$= \ln R_1. \tag{17}$$

This proves the stability of our method clearly. Compared with the traditional Tang's model, the inhomogeneous plasma case can be also dealt with in our model. Besides, our model exhibits much higher efficiency than the DEPLETE model (Strozzi et al., 2008) since the solving of a two-point boundary value problem via a shooting method is avoided.

Numerical results

In order to demonstrate the validity of our model, the typical numerical results are presented in this section. The plasma and laser parameters in experiments conducted by Montgomery et al. (1998) are considered. A uniform 1 mm plasma, consisting of 50% C_3H_8 and 50% C_5H_{12}, is generated before the incidence of pump laser ($I_0 = 2 \times 10^{15}$ W/cm², $\lambda_0 = 351$ nm). The electron temperature is heated to $T_e \approx 3$ keV, while the ion temperature keeps as $T_i = T_e/3$. The electron density of the plasma varies from 0.05 to $0.15 n_c$ for different calculating cases, where $n_c = \omega_0^2 \varepsilon_0 m_e/e^2$ denotes the critical density of the pump laser. Hereafter, we choose the above plasma and laser parameters as default input condition to calculate the linear gain exponent, reflectivity, and distribution of backscattered light.

Figure 2 shows the gain exponent of SRS as a function of the scattered light frequency for different electron densities. One should notice that we take the above method in steady state to apply independently at each scattered frequency. This may be viewed as a "completely incoherent" treatment of the scattered light at different frequencies. The maximum gain of SRS appears at the frequency where the three-wave-coupling condition is exactly satisfied. Besides, the maximum gain of SRS increases with the electron density, which is consistent with the traditional linear theory (Froula et al., 2010). Furthermore, with the increase of the electron density, the gain peak moves to lower frequencies, and narrows. The narrowing in frequency with increased electron density is mainly due to the enhancement of the three-wave-coupling.

The gain exponent of SBS as a function of the scattered light frequency is displayed in Figure 3. Compared with that of the
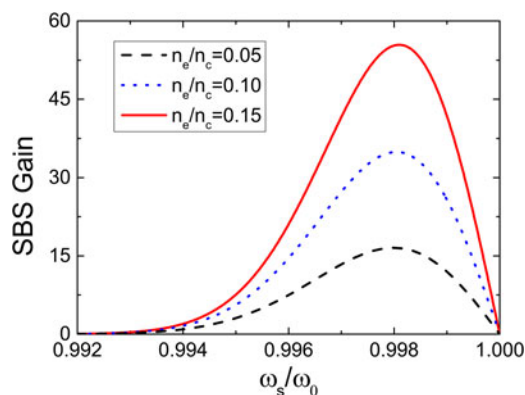
Fig. 3. The gain exponent of SBS as a function of the scattered light frequency (normalized by the pump laser frequency ω_0) for $n_e/n_c = 0.05$ (black dashed), $n_e/n_c = 0.1$ (blue dotted), and $n_e/n_c = 0.15$ (red solid), respectively.

Fig. 5. Maximum gain of both SRS (red solid) and SBS (blue dashed) versus the electron temperature with $n_e/n_c = 0.1$.
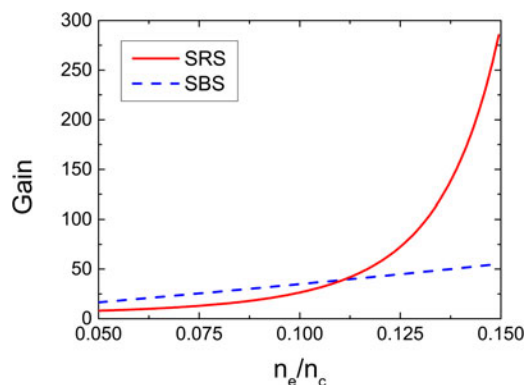

Fig. 4. Maximum gain of both SRS (red solid) and SBS (blue dashed) versus the electron density with electron temperature $T_e = 3$ keV.

SRS, the general SBS gain peak is much narrower (note that the range of x coordinator axis is much smaller than that in Fig. 2), and the maximum also increases with the electron density as well. Because of the small frequency of ion acoustic wave, the spectral width of SBS gain keeps almost the same. For the low-density case ($n_e/n_c = 0.05$), the maximum SBS gain (16.5) is higher than the SRS (8.1). However, with the increase of electron density, the maximum SRS gain rises rapidly and will become five times of the SBS for the high-density case ($n_e/n_c = 0.15$).

In order to investigate the dependence of the gains on the electron density quantitatively, we focus on the maximum gain. Figure 4 presents the maximum gain of both SRS and SBS versus the electron density with electron temperature $T_e = 3$ keV. The maximum SBS gain exhibits linear dependence on the electron density, while the maximum SRS gain increases exponentially with the electron density. The maximum SRS gain exceeds the SBS at the density of $n_e/n_c = 0.11$. Physically, for the SRS, the Landau damping of the Langmuir wave is very sensitive to the electron density and decreases significantly with the increase of electron density. However, for the SBS, the Landau damping of the ion acoustic wave keeps almost the same, so the maximum SBS gain scales linearly with the electron density. Our calculation is consistent with the results given by Gong *et al.* (2013).

The dependence of the maximum gain on the electron temperature with $n_e/n_c = 0.1$ is exhibited in Figure 5. For both SRS and SBS, the maximum gain reduce noticeably with the electron
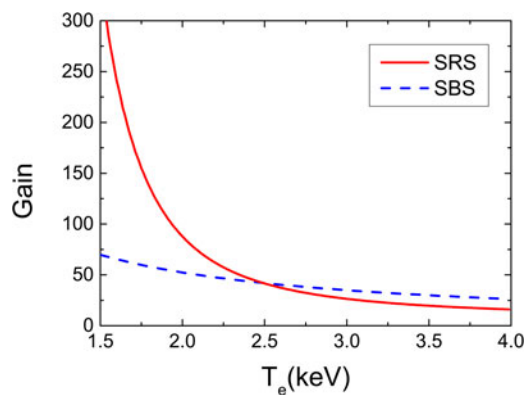
temperature. Compared with the SBS, the maximum gain of SRS drops much more intensely. Above the temperature of $T_e = 2.5$ keV, the maximum gain of SRS becomes smaller than the SBS. For the SBS, the Landau damping of the ion acoustic wave rises with the electron temperature, which results in the deduction of the maximum gain. While, for the SRS, the Landau damping of the Langmuir wave is mainly determined by the Debye length of electrons $\lambda_{De} = v_{te}/\omega_{pe}$. With higher electron temperature, the Debye length of electrons becomes larger. Thus, the maximum gain of SRS decreases with electron temperature significantly. This indicates that by increasing the electron temperature, one can effectively suppress the gain of both SRS and SBS in ICF.

The spatial intensity distributions of pump laser and the back-scattered light of both SRS and SBS are shown in Figure 6. Two different electron density cases are compared with each other: (a) the low-density case ($n_e/n_c = 0.05$) and (b) the high-density case ($n_e/n_c = 0.15$). The scattered intensities are integrated by all frequencies of the backscattered light. For the low-density case (see Fig. 6a), the intensity of pump laser (green solid) keeps almost constant all over the whole interaction region. While both SRS (red dashed) and SBS (blue dotted) are driven slightly since the gains of both SRS and SBS are small as shown in Figures 2 and 3. The SBS dominates the scattering process in the low-density case because the maximum SBS gain is nearly twice the value of SRS as mentioned above. For the high-density case (see Fig. 6b), the pump laser is depleted obviously because of the large linear gains of SRS and SBS. Different from the low-density case, the SRS exhibits much higher reflectivity than the SBS due to its higher gain. Furthermore, the gain of SRS is more sensitive to electron density than that of the SBS, and the ratio of SRS intensity to SBS intensity increases drastically with electron density. One should notice that the pump depletion is self-consistently included in our model. Thus, considering the coexistence of the SRS and SBS processes, the denser the plasma is, the more significantly the SBS is suppressed.

Nonlinear saturation and competition between SRS and SBS

Our model has the capability to calculate the reflectivities of both SRS and SBS simultaneously. However, the reflectivity is calculated based on the linear gain exponent by Eq. (11), and nonlinear saturation mechanisms, such as decay instability of daughter waves (Labaune *et al.*, 1998; Depierreux *et al.*, 2002), wave
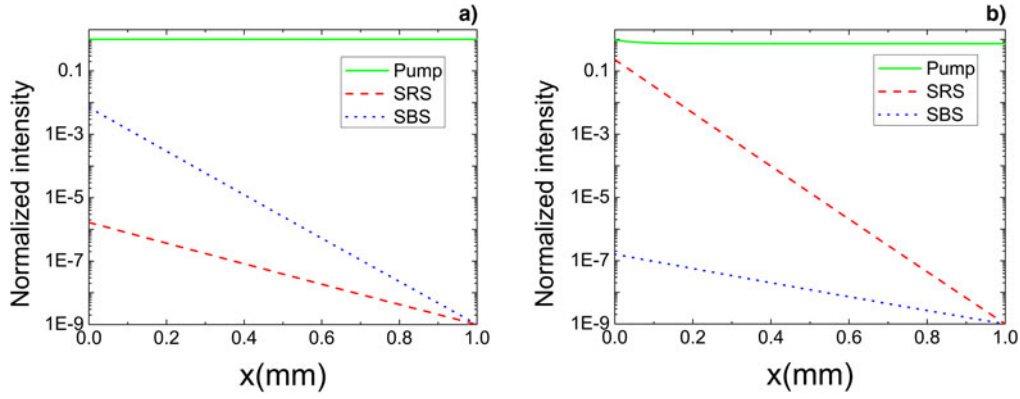
Fig. 6. Spatial intensity distributions of pump laser (green solid) and the backscattered light of both SRS (red dashed) and SBS (blue dotted) for two different electron densities: (a) $n_e/n_c = 0.05$ and (b) $n_e/n_c = 0.15$. The intensities are normalized by the intensity of pump laser at the left boundary.

breaking (Forslund et al., 1975), and nonlinear frequency shift due to particle trapping (Morales and O'Neil, 1972; Divol et al., 2003), are not included in the model. A detailed discussion of the nonlinear saturation mechanisms is beyond the scope of this paper. Whereas, neglecting of the nonlinear saturation mechanisms may lead to an overestimate of the final reflectivity. In order to make the model be able to calculate the reflectivity reasonably, a phenomenological method is proposed to include the nonlinear saturation mechanisms in our model. The nonlinear saturation mechanisms mentioned above mitigate the growth of backscattered light by saturating its gain exponent, so that a threshold for the gain exponent G_{th} is introduced in our model. According to the relevant results of experiments (Lindl et al., 2004), we set $G_{th} = 30$, then the gain exponent G is revised as

$$G' = \frac{G G_{th}}{\sqrt[10]{G^{10} + G_{th}^{10}}}. \tag{18}$$

This revision form guarantees that for small G ($G \leq 10$), the revision is negligible, while for large G ($G \geq 30$), the gain exponent is restrict to G_{th}. Traditional theory shows that the backscattered light extracts energy from the pump laser and grows quickly from the noise level up to its maximum (Kruer, 1988; Lindl et al., 2004). Although the pump depletion is self-consistently included in our model, the competition between SRS and SBS should be also considered in the model. Thus, the gain exponents of SRS and SBS are further revised as

$$G'_{SRS} = \frac{G_{SRS} G_{th}}{\sqrt[10]{G_{SRS}^{10} + G_{SBS}^{10} + G_{th}^{10}}}, \tag{19}$$

$$G'_{SBS} = \frac{G_{SBS} G_{th}}{\sqrt[10]{G_{SRS}^{10} + G_{SBS}^{10} + G_{th}^{10}}}, \tag{20}$$

respectively. G_{SRS} and G_{SBS} denote the initial gain exponents derived from Eq. (10). For small gain exponents, the above revisions are negligible. However, when the gain exponents of SRS and SBS become noticeable, the larger one will suppress the smaller one significantly according to Eqs (19) and (20).

To illustrate the influences of nonlinear saturation and competition effect on the SRS and SBS processes, reflectivities of both SRS and SBS versus normalized electron density are presented in
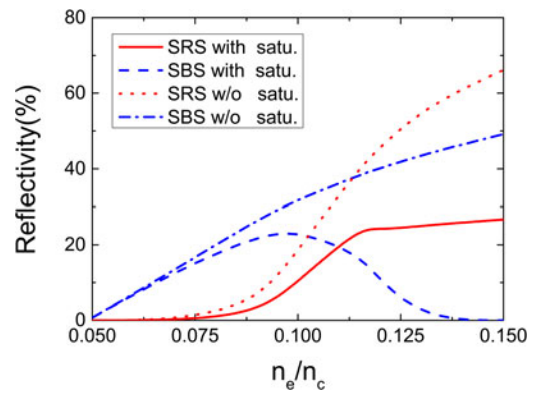

Fig. 7. Reflectivities of both SRS (red) and SBS (blue) versus normalized electron density with (solid, dashed) and without (dotted, dotted-dashed) nonlinear saturation and competition effect.

Figure 7. Parameters of the pump laser and the plasma are the same as that used in Figure 4. It is seen that, without the nonlinear saturation effect, the sum of the SRS (red dotted) and SBS (blue dotted-dashed) reflectivities exceeds the intensity of pump laser beyond the intensity of $n_e/n_c = 0.13$, which is unphysical. Obviously, the nonlinear saturation effect suppresses the gain of the SRS and SBS processes significantly; therefore, the sum of the reflectivities of SRS (red solid) and SBS (blue dashed) are restricted to a reasonable value. Furthermore, without the nonlinear saturation and competition effect, the reflectivities of both SRS and SBS increase with the electron density monotonically. However, considering the nonlinear saturation and competition effect, totally different trend appears. On the one hand, the SRS reflectivity (red solid) tends to be saturated when the electron density becomes higher than $n_e/n_c = 0.115$. On the other hand, the SBS reflectivity does not continuously grow with the electron density any more. Instead, it keeps increasing with the electron density until $n_e/n_c = 0.95$, then it starts to decrease with the electron density. Compared with the SRS, the SBS reflectivity is negligible for a high-density case. The typical anti-correlation between SRS and SBS versus electron density observed in experiments (Montgomery et al., 1998) is reproduced in our model, which proves the effectiveness of the phenomenological method utilized in our model.

In order to investigate the efficiency and accuracy of our model, two typical experimental results from the OMEGA laser
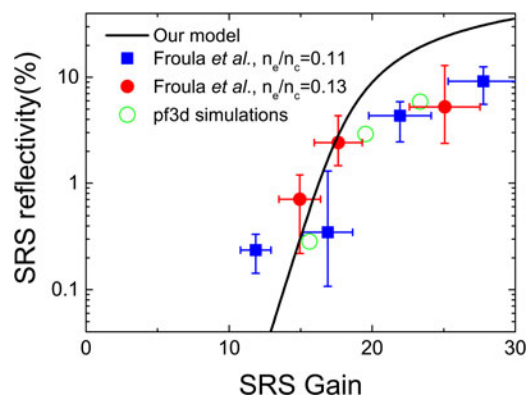
Fig. 8. Theoretical SRS reflectivity as a function of the gain exponent, compared with the experimental and simulation results from Froula *et al.* (2010) for different electron densities.
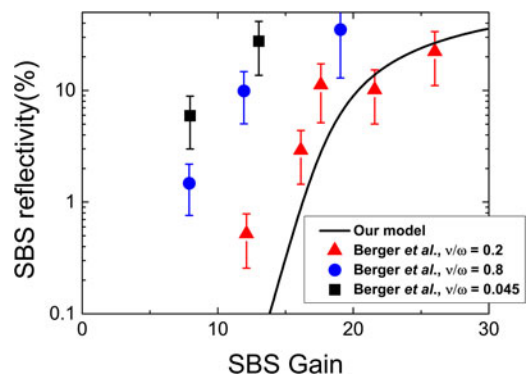

Fig. 9. Theoretical SBS reflectivity as a function of the gain exponent, compared with the experimental data from Berger *et al.* (2015) for various Landau damping rates of ion acoustic wave (υ/ω).

facility (Soures *et al.*, 1996) are chosen to be compared with our model for SRS and SBS, respectively. Figure 8 presents the theoretical SRS reflectivity as a function of the gain exponent by our model, compared with the experimental and simulation results from Froula *et al.* (2010). In the experiments, the electron density is scaled in the 2-mm-long target platform from 0.11 to $0.13n_c$, maintaining the electron temperature above 2.5 keV. The reflectivity is calculated after the rise of the heating laser beams (1.2 ns, 1×10^{15} W/cm^2, 351 nm) by averaging over a 100 ps range. Hydrodynamic simulations by using the pf3d code (Berger *et al.*, 1998) are also performed. Generally, our calculation is in agreement with the results of the experiments and simulations, which indicates that our model can qualitatively reveal the SRS reflectivity. However, the overestimate of the reflectivity for the high gains reflects the lack of the multidimensionality of the real instability process in our model.

Comparison of our model calculation with the experimental results by Berger *et al.* (2015) for the SBS is exhibited in Figure 9. In the experiments, the laser intensity, approximately constant with a 1ns pulse length, is varied between 2.2×10^{14} and 8.8×10^{14} W/cm^2. The 2-mm-long hohlraum is filled with 1 atm of CO_2, which yields an electron density of $n_e/n_c = 0.06$. The electron temperature reaches the peak value of 3.5 keV. The ion Landau damping rate is varied by adding hydrogen to the CO_2 hohlraum gas fill. As shown in Figure 9, the symbols with

different colors represent the SBS reflectivities measured for different Landau damping rates of the ion acoustic wave. The black solid line is the calculation result of our model. Obviously, the experimental results are qualitatively reproduced by our model. Besides, the result of experiments shows that increasing ion Landau damping can strongly suppress the SBS. However, due to the strong damping limit of our model, deviation from the experimental results exists in the small damping cases, which means that our model is not valid under the small damping condition.

Conclusion

A one-dimensional steady-state model for the SRS and SBS process in laser-plasma interaction is developed. The model can calculate the reflectivities of SBS and SRS simultaneously with a "completely incoherent" treatment of the scattered light at different frequencies. Compared with the traditional Tang's model (Divol *et al.*, 2003), the inhomogeneous plasma case can be also dealt with in our model. Furthermore, due to the novel "predictor-corrector" method, the solving of a two-point boundary value problem via a shooting method in the DEPLETE model (Strozzi *et al.*, 2008) is avoided. Based on the model, the influences of the electron density and temperature on the gains of both SRS and SBS are investigated, which indicates that the SRS gain is more sensitive to the electron density and temperature than that of the SBS. Spatial intensity distributions of the pump laser and the backscattered light demonstrates that for the low-density case, the SBS dominates the scattering process, while the SRS exhibits much higher reflectivity than the SBS in the high-density case. To include the nonlinear saturation mechanisms and competition between SRS and SBS in our model, a phenomenological method is proposed. The typical anti-correlation between SRS and SBS versus electron density observed in experiments (Montgomery *et al.*, 1998) is reproduced in our model, which proves the effectiveness of the phenomenological method. Two typical experimental results from the OMEGA laser facility (Soures *et al.*, 1996) are compared with our calculation for SRS and SBS, respectively. The calculation results qualitatively reveal the SRS and SBS reflectivities. However, due to the lack of the multidimensionality and the strong damping limit in our model, deviation from the experimental results does exist. Besides, our model can not handle the ultra-short laser pulse case, for which the steady-state assumption is not valid. In spite of the limitations, our model exhibits robustness and efficiency in a wide range of situations, which will be promising for the hydrodynamic simulation and theoretical quick analysis of the ICF experiments.

References

Abramowitz M and Stegun IA (1970) *Handbook of Mathematical Functions: With Formulas, Graphs, and Mathematical Tables*. New York: Dover.

Amiranoff F, Riconda C, Chiaramello M, Lancia L, Marqués JR and Weber S (2018) The role of the globe phase in the spatio-temporal evolution of strong-coupling Brillouin scattering. *Physics of Plasmas* **25**, 013114.

Berger RL, Still CH, Williams EA and Langdon AB (1998) On the dominant and subdominant behavior of stimulated Raman and Brillouin scattering driven by nonuniform laser beams. *Physics of Plasmas* **5**, 4337.

Berger RL, Suter LJ, Divol L, London RA, Chapman T, Froula DH, Meezan NB, Neumayer P and Glenzer SH (2015) Beyond the gain exponent: effect of damping, scale length, and speckle length on stimulated scatter. *Physical Review E* **91**, 031103.

Boyd TJM and Sanderson JJ (2003) *The Physics of Plasmas*. Cambridge University Press.

Depierreux S, Labaune C, Fuchs J, Pesme D, Tikhonchuk VT and Baldis HA (2002) Langmuir decay instability cascade in laser-plasma experiments. *Physical Review Letters* **89**, 045001.

Divol L, Berger RL, Cohen BI, Williams EA, Langdon AB, Lasinski BF, Froula DH and Glenzer SH (2003) Modeling the nonlinear saturation of stimulated Brillouin backscatter in laser heated plasmas. *Physics of Plasmas* **10**, 1822.

Forslund DW, Kindel JM and Lindman EL (1975) Plasma simulation studies of stimulated scattering processes in laser-irradiated plasmas. *Physics of Fluids* **18**, 1017.

Fried BD and Conte SD (1961) *The Plasma Dispersion Function: The Hilbert Transform of the Gaussian*. New York: Academic.

Froula DH, Divol L, London RA, Berger RL, Doppner T, Meezan NB, Ralph J, Ross JS, Suter LJ and Glenzer SH (2010) Experimental basis for laser-plasma interactions in ignition hohlraums at the National Ignition Facility. *Physics of Plasmas* **17**, 056302.

Glenzer SH, MacGowan BJ, Meezan NB, Adams PA, Alfonso JB, Alger ET, Alherz Z, Alvarez LF, Alvarez SS and Amick PV (2011) Demonstration of ignition radiation temperatures in indirect-drive inertial confinement fusion hohlraums. *Physical Review Letters* **106**, 085004.

Gong T, Li ZC, Zhao B, Hu GY and Zheng J (2013) Noise sources and competition between stimulated Brillouin and Raman scattering: a one-dimensional steady-state approach. *Physics of Plasmas* **20**, 092702.

Hao L, Liu ZJ, Zheng CY, Xiang J, Feng W, Hu XY and Li B (2012) Study of stimulated Raman and Brillouin scattering in a finite interaction region under the convective instability condition. *Chinese Science Bulletin* **57**, 2747.

Hao L, Zhao YQ, Yang D, Liu ZJ, Hu XY, Zheng CY, Zou SY, Wang F, Peng XS, Li ZC, Li SW, Xu T and Wei HY (2014) Analysis of stimulated Raman backscatter and stimulated Brillouin backscatter in experiments performed on SG-III prototype facility with a spectral analysis code. *Physics of Plasmas* **21**, 072705.

Hinkel DE, Callahan DA, Langdon AB, Langer SH, Still CH and Williams EA (2008) Analyses of laser-plasma interactions in National Ignition Facility ignition targets. *Physics of Plasmas* **15**, 056314.

Hu YM and Hu XW (2003) Parametric processes of a strong laser in partially ionized plasmas. *Physical Review E* **67**, 036402.

Kirkwood RK, Turnbull SP, Chapman T, Wilks SC, Rosen MD, London RA, Pickworth LA, Colaitis A, Dunlop WH, Poole P, Moody JD, Strozzi SJ, Michel PA, Divol L, Landen OL, MacGowan BJ, Van Wonterghem BM, Fournier KB and Blue BE (2018) A plasma amplifier to combine multiple beams at NIF. *Physics of Plasmas* **25**, 056701.

Kruer WL (1988) *The Physics of Laser Plasma Interactions*. Redwood City, CA: Addison-Wesley Publishing Co.

Labaune C, Baldis HA, Bauer BS, Tikhonchuk VT and Laval G (1998) Time-resolved measurements of secondary Langmuir waves produced by the Langmuir decay instability in a laser-produced plasma. *Physics of Plasmas* **5**, 234.

Li ZC, Zheng J, Jiang XH, Wang ZB, Yang D, Zhang H, Li SW, Yin Q, Zhu FH, Shao P, Peng XS, Wang F, Guo L, Yuan P, Yuan Z, Chen L, Liu SY, Jiang SE and Ding YK (2012) Interaction of 0.53 µm laser pulse with millimeter-scale plasmas generated by gasbag target. *Physics of Plasmas* **19**, 062703.

Lindl JD (1998) *Inertial Confinement Fusion: The Quest for Ignition and Energy Gain Using Indirect Drive*. American Institute of Physics.

Lindl JD, Amendt P, Berger RL, Glendinning SG, Glenzer SH, Haan SW, Kauffman RL, Landen OL and Suter LJ (2004) The physics basis for ignition using indirect-drive targets on the National Ignition Facility. *Physics of Plasmas* **11**, 339.

Marqués JR, Lancia L, Gangolf T, Blecher M, Bolaños S, Fuchs J, Willi O, Amiranoff F, Berger RL, Chiaramello M, Weber S and Riconda C (2019) Joule-level high-efficiency energy transfer to subpicosecond laser pulses by a plasma-based amplifier. *Physical Review X* **9**, 021008.

Montgomery DS, Afeyan BB, Cobble JA, Fernandez JC, Wilke MD, Glenzer SH, Kirkwood RK, MacGowan BJ, Moody JD, Lindman EL, Munro DH, Wilde BH, Rose HA, Dubois DF, Bezzerides B and Vu HX (1998) Evidence of plasma fluctuations and their effect on the growth of stimulated Brillouin and stimulated Raman scattering in laser plasmas. *Physics of Plasmas* **5**, 1973.

Morales GJ and O'Neil TM (1972) Nonlinear frequency shift of an electron plasma wave. *Physical Review Letters* **28**, 417.

Neumayer P, Berger RL, Divol L, Froula DH, London RA, MacGowan BJ, Meezan NB, Ross JS, Sorce C, Suter LJ and Glenzer SH (2008) Suppression of stimulated Brillouin scattering by increased Landau damping in multiple-ion-species hohlraum plasmas. *Physical Review Letters* **100**, 105001.

Peng H, Marqués JR, Lancia L, Amiranoff F, Berger RL, Weber S and Riconda C (2019) Plasma optics in the context of high intensity lasers. *Matter and Radiation at Extremes* **4**, 065401.

Pesme D, Laval G and Pellat R (1973) Parametric instabilities in bounded plasmas. *Physical Review Letters* **31**, 203.

Powers LV, Berger RL, Kauffman RL, MacGowan BJ, Amendt PA, Back CA, Bernat TP, Dixit SN, Eimer DI and Estabrook KG (1995) Gas-filled targets for large scale-length plasma interaction experiments on Nova. *Physics of Plasmas* **2**, 2473.

Ramani A and Max CE (1983) Stimulated Brillouin scattering in an inhomogeneous plasma with broad-bandwidth thermal noise. *Physics of Fluids* **26**, 1079.

Rosenbluth MN (1972) Parametric instabilities in inhomogeneous media. *Physical Review Letters* **29**, 565.

Soures JM, McCrory RL, Verdon CP, Babushkin A, Bahr RE, Boehly TR, Boni R, Bradley DK, Brown DL and Craxton RS (1996) Direct-drive laser-fusion experiments with the OMEGA, 60-beam, >40 kJ, ultraviolet laser system. *Physics of Plasmas* **3**, 2108.

Strozzi DJ, Williams EA, Hinkel DE, Froula DH, London RA and Callahan DA (2008) Ray-based calculations of backscatter in laser fusion targets. *Physics of Plasmas* **15**, 102703.

Tang CL (1966) Saturation and spectral characteristics of the Stokes emission in the stimulated Brillouin process. *Journal of Applied Physics* **37**, 2945.